JACS
JOURNAL OF THE AMERICAN CHEMICAL SOCIETY
Article
pubs.acs.org/JACS

Reductive Cleavage of Nitrite to Form Terminal Uranium Mono-Oxo Complexes

Andrew J. Lewis, Patrick J. Carroll, and Eric J. Schelter*

P. Roy and Diana T. Vagelos Laboratories, Department of Chemistry, University of Pennsylvania, 231 South 34th Street, Philadelphia, Pennsylvania 19104, United States

Supporting Information

ABSTRACT: Uranium terminal mono-oxo complexes are prepared with a unique activation of nitrite following reductive cleavage of an N−O bond with loss of nitric oxide. The thermodynamic driving force of U═O bond formation differentiates this reactivity from known mechanisms of nitrite reduction, which are typically mediated by proton transfer. Mechanistic details are explored by DFT supporting a simple homolytic cleavage pathway from a κ^1−ONO bound intermediate. Complexes of the formula $U^{VI}OX[N(SiMe_3)_2]_3$ are formed providing a trigonal bipyramidal framework into which ligands trans to the U═O bond may be installed.

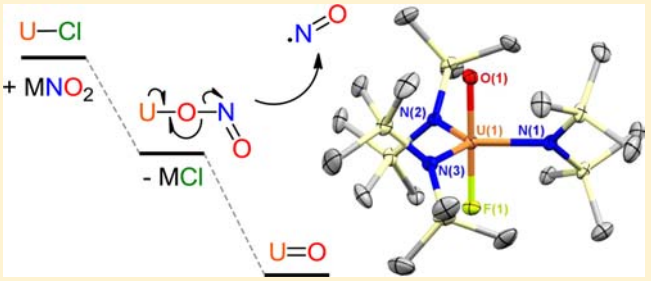

INTRODUCTION

The one-electron reduction of nitrite (NO_2^-) to form nitric oxide (NO) is a critical reaction in denitrification.[1] This reaction is catalyzed by iron- or copper-containing nitrite reductase (NiR) enzymes that are present in anaerobic bacteria. Synthetic work directed toward understanding this reactivity has focused primarily on Cu-complexes that reduce nitrite under biologically relevant conditions.[2−5] Fe−NO_2 complexes can be deoxygenated by PPh_3 to form biologically relevant dinitrosyl iron complexes (DNICs).[6,7] Metalloporphyrin nitrite complexes, M = Mn,[8] Fe,[8] Cr,[9] or Mo,[10] undergo N−O bond cleavage upon UV photolysis to generate metal-oxo complexes, a reaction that occurs in reverse in the case of $[Fe^{IV}O(tmc)(OAc)]^+$ (tmc =1,4,8,11-tetramethyl-1,4,8,11-tetraazacyclotetradecane), where NO adds to form a transiently stable Fe^{III}-nitrite complex.[11] In contrast, the reactivity of lanthanide− and actinide−nitrite complexes has received little attention amidst numerous recent examples of activation of other small molecules with these elements.[12,13]

Methods for activating small molecules with uranium have focused on multielectron reduction chemistry using electropositive, low-, and midvalent ions. These reactions often lead to the formation of uranium-ligand multiple bonds.[14] A rare example of small molecule activation using high-valent uranium is found in the metathesis of a U^V−imido complex with CO_2 to generate a uranium−oxo complex and an isocyanide.[15] We reasoned that high valent uranium could similarly affect unique reactivity in nitrite reduction through single electron transfer reminiscent of copper complexes but driven by U═O bond formation. Here, we report that uranium(IV) and uranium(V) complexes reductively cleave nitrite anions to selectively replace a U−X bond with an oxo ligand.

The one-electron reduction of nitrite by uranium(V) is a general route to terminal uranium mono-oxo complexes, which have been of considerable interest recently.[14,16−18] Importantly, the nitrite activation methodology can be controlled to avoid the formation of uranyl (UO_2^{2+}) complexes, which are a major thermodynamic sink in the coordination chemistry of uranium. The uranium(VI) mono-oxo complexes that have been isolated in the present work provide a unique opportunity to compare the electronic structures of uranyl with uranium(VI) terminal mono-oxo complexes in a conserved structural framework. In contrast to the reactivity of nitrite with transition metals, the reactions with uranium proceed at room temperature in the absence of a proton source, without the need for photolysis or additional reagents for oxygen atom abstraction.

RESULTS AND DISCUSSION

Synthesis/Characterization. We recently reported a methodology for the synthesis of several pentavalent uranium trans-dihalides of the formula $U^VX_2[N(SiMe_3)_2]_3$ (X = F^-, Cl^-, Br^-).[19] We hypothesized that reaction of small molecules with the uranium complexes containing favorable leaving groups in the axial positions could induce unusual reactivity. Indeed, upon treating $U^VCl_2[N(SiMe_3)_2]_3$ with $NaNO_2$ in THF a color change of the reaction mixture from dark red to dark green was observed. Analysis of the product mixture revealed that no characteristic nitrite stretching bands could be identified by IR spectroscopy and no new paramagnetically shifted products could be observed in the ^1H NMR spectrum. X-ray structural analysis revealed the product of this reaction to be $U^{VI}OCl[N(SiMe_3)_2]_3$ (**1**) (Figure 1). The X-ray structure of **1** revealed

Received: November 9, 2012
Published: December 6, 2012

dx.doi.org/10.1021/ja311057y | J. Am. Chem. Soc. 2013, 135, 511−518

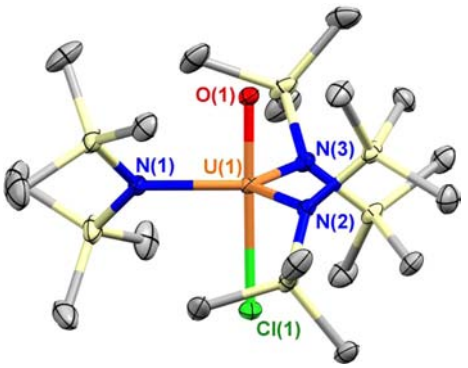

Figure 1. Thermal ellipsoid plot of **1** at 30% probability. Hydrogen atoms are omitted for clarity. Bond lengths (Å) and angles (deg): U(1)−O(1) 1.803(5), U(1)−O(1′) 1.788(8), U(1)−Cl(1) 2.5369(17), U(1)−Cl(1′) 2.546(3), U(1)−N(1) 2.196(2), U(1)−N(2) 2.193(2), U(1)−N(3) 2.191(2), O(1)−U(1)−Cl(1) 179.27(11), O(1′)−U(1)−Cl(1′) 178.6(2). The O(1) and Cl(1) atoms are disordered over the two axial positions.

a trigonal bipyramidal geometry in which mixed occupancy of the oxo- and chloro- ligand was observed at both sites. The product was isolated in 74% yield following recrystallization from $(Me_3Si)_2O$ (Scheme 1). This reaction represents the first example of a uranium(VI) terminal mono-oxo formed from a uranium(V)−halide complex.

Scheme 1. Synthesis of Terminal Uranium(VI) Mono-Oxo Complexes from Reaction with Nitrite

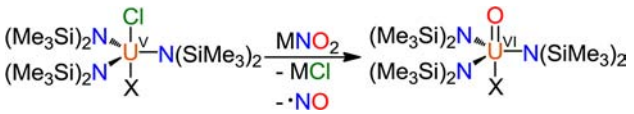

Traditional methods to synthesize uranium mono-oxo complexes have focused on two-electron oxidation of uranium(III) or uranium(IV) precursors, with oxygen atom transfer reagents such as pyridine *N*-oxide, trimethylamine *N*-oxide, *N*-methylmorpholine-*N*-oxide, and 2,2,6,6-tetramethylpiperidine *N*-oxide.[18,20−25] Uranium mono-oxo complexes have also been prepared by double bond metathesis between uranium-imido complex and CO_2,[15] and through selective protonation of a single oxo ligand of uranyl.[26] The synthesis of **1** was also possible through the use of $AgNO_2$ without visible formation of Ag^0 proceeding over a shorter reaction time and in comparable yield. The increased reactivity of $AgNO_2$ toward $U^{V}Cl_2[N(SiMe_3)_2]_3$ is likely due to the higher lattice energy of AgCl than NaCl at 217 versus 184 kcal/mol, respectively.[27]

The ^{1}H NMR spectrum of **1** exhibits two sharp resonances at 0.55 and 0.61 ppm in benzene-d_6 in a 1:1 ratio due to the different chemical environments in each axial direction from the trigonal plane of the molecule. The appearance of two peaks at room temperature indicates hindered rotation about the U−N bonds caused by the collective arrangement of the bulky $-SiMe_3$ groups.[28] The U═O stretching peak was identified in the IR spectrum at 862 cm^{-1}, however this mode overlaps with strong vibrations from the amide ligands, supported by DFT calculations (vide infra).

Having isolated **1** directly through two routes from a uranium(V)-chloride precursor we next sought to expand the nitrite activation methodology to other uranium oxidation states. Complex **1** was similarly accessed by an alternative,

Scheme 2. Synthesis of Uranium(VI) Terminal Mono-Oxo Complexes through Various Routes; (a) Fluoranil, Et_2O, (b) *N*-Methylmorpholine-*N*-oxide, Et_2O

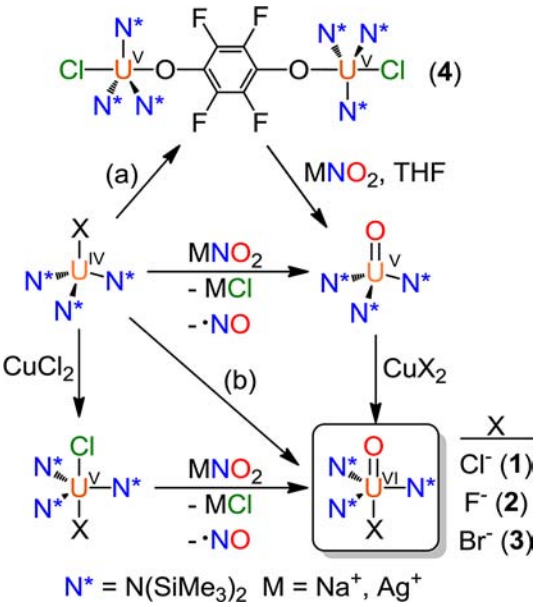

stepwise pathway (Scheme 2). Addition of $AgNO_2$ to $U^{IV}Cl[N(SiMe_3)_2]_3$ in THF led to the formation of the known complex $U^{V}O[N(SiMe_3)_2]_3$,[24,29] in an unprecedented direct oxidation of a uranium(IV) complex to a uranium(V)-oxo product. Subsequent oxidation of $U^{V}O[N(SiMe_3)_2]_3$ with $CuCl_2$ produced **1**. Additionally, **1** could be prepared in a two-electron oxidation from the addition of *N*-methylmorpholine-*N*-oxide to $U^{IV}Cl[N(SiMe_3)_2]_3$.

In the reaction of $U^{V}Cl_2[N(SiMe_3)_2]_3$ with NO_2^-, longer reaction times led to the formation of yellow $U^{VI}O_2[N(SiMe_3)_2]_2(THF)_2$ as a side product, which was identified by comparison of the ^{1}H NMR spectrum of the reported compound and confirmed by X-ray crystallography.[30,31] Complete conversion to the uranyl product was observed after two days in the presence of excess NO_2^-. The absence of available valence electrons on uranium in **1** implies that the second nitrite reduction occurs by means of oxidation of an $N(SiMe_3)_2^-$ ligand to the highly unstable bis(timethylsilyl)-aminyl radical. The aminyl radical is known to elicit hydrogen atom abstraction from ethereal solvents to generate $HN(SiMe_3)_2$.[32] Indeed, the free amine $HN(SiMe_3)_2$ was detected by ^{1}H NMR as a product of the second oxidation reaction. Homolytic cleavage of a $M-N(SiMe_3)_2$ bond has been proposed in the one-electron reduction of a uranyl complex previously.[33] This second oxidation pathway was not observed when the reactions were performed in Et_2O suggesting that uranyl formation is promoted in THF.

We expected that inhibiting the second nitrite substitution step would preclude uranyl formation. To test this hypothesis, we employed the uranium(V) complex $U^{V}ClF[N(SiMe_3)_2]_3$, which has one chloride ligand and one fluoride ligand in the axial positions. Our hypothesis was that addition of 1 equiv of nitrite anion to $U^{V}ClF[N(SiMe_3)_2]_3$ would preferentially form a mono-oxo complex. Reaction of $U^{V}ClF[N(SiMe_3)_2]_3$ with $AgNO_2$ in Et_2O led to the formation of the expected product $U^{VI}OF[N(SiMe_3)_2]_3$ (**2**). The corresponding reaction of $U^{V}ClF[N(SiMe_3)_2]_3$ with $NaNO_2$ also led to formation of **2** without the generation of uranyl; however, this reaction

dx.doi.org/10.1021/ja311057y | J. Am. Chem. Soc. 2013, 135, 511−518

proceeded more slowly than the similar reaction to form **1**. An inverse trans effect of the U−Cl bond by the stronger U−F bond likely limits the rate of nitrite substitution and the utility of this pathway. Similar to **1**, treatment of $UF[N(SiMe_3)_2]_3$ with *N*-methylmorpholine-*N*-oxide also cleanly generated **2**.

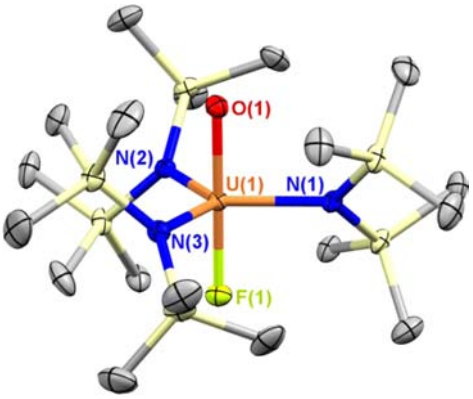

Figure 2. Thermal ellipsoid plot of **2** at 30% probability. Hydrogen atoms are omitted for clarity. Bond lengths (Å) and angles (deg): U(1)−O(1) 1.9198(16), U(1)−F(1) 1.9246(16), U(1)−N(1) 2.210(2), U(1)−N(2) 2.2060(19), U(1)−N(3) 2.2090(19), F(1)−U(1)−O(1) 179.07. U−F and U−O bond lengths are unreliable due to partial occupancy of these two atoms in the two axial positions.

The ^{1}H NMR spectrum of **2** was similar to that of **1**, with two sharp resonances in a 1:1 ratio. The ^{19}F NMR spectrum displayed a single peak at 586.8 ppm versus $CFCl_3$. ^{19}F NMR data for molecules containing U^{VI}−F bonds are rare and useful for the calibration of theoretical methods; compounds of the formula UF_nCl_{6-n} exhibit resonances between +750−790 ppm,[34] in which the shift is dependent on the nature of the trans U−F/Cl bonding.[35] In the IR spectrum of **2**, the U═O stretch was identified at 882 cm^{-1}, about 20 cm^{-1} higher in energy than that of **1**, consistent with a greater inverse trans influence stabilization by fluoride than chloride. A similar comparison of *trans*-fluoro versus *trans*-oxo ligand substitution on the energies of U−F stretching modes has been noted previously.[36]

Attempts to form the analogous uranium−oxo−bromide complex from the reaction of $U^{V}Br_2[N(SiMe_3)_2]_3$ with nitrite were unsuccessful due to the rapid substitution of bromide with nitrite leading to facile uranyl formation even at low temperature. However, addition of *N*-methylmorpholine-*N*-oxide to $U^{IV}Br[N(SiMe_3)_2]_3$ produced $U^{VI}OBr[N(SiMe_3)_2]_3$ (**3**). The structure of **3** was confirmed by X-ray diffraction of a single crystal obtained from recrystallization from pentane. The IR spectrum of **3** showed a U═O stretching peak at 859 cm^{-1} at slightly lower energy than that of **1**.

Having observed the ability for homolysis of a $U-N(SiMe_3)_2$ bond to induce nitrite reduction, we were interested in whether a deliberate ligand-based redox event could be exploited to reduce nitrite in a controlled fashion. Addition of *p*-fluoranil (FA, tetrafluoro-1,4-benzoquinone) to 2 equiv $U^{IV}Cl[N(SiMe_3)_2]_3$ led to an immediate color change from pale tan to dark brown. Recrystallization from pentane afforded $\{U^{V}Cl[N(SiMe_3)_2]_3\}_2(\mu_2\text{-FA})$ (**4**) as a black solid. Structural analysis, IR spectroscopy, near-IR absorption spectroscopy, and solution electrochemistry support the presence of two uranium(V) ions in the complex that are bridged by a tetrafluoro-*p*-phenylenediolate. The diolate ligand in **4** is the product of doubly reduced FA (Supporting Information).

Multiple overlapping peaks between −3 and 0 ppm are present in the ^{1}H NMR spectrum of **4** due to the large steric demand of the axial ligands and the different chemical environment on each face of the complex. The resonances between −3 and 0 ppm coalesce into two broad peaks above 45 °C, centered at −0.74 and −1.16 ppm. A single paramagnetically shifted peak was observed in the ^{19}F NMR spectrum at room temperature. Addition of 2 equiv $NaNO_2$ to **4** in THF led to formation of $U^{V}O[N(SiMe_3)_2]_3$ as the major product. Although this reaction formally proceeds through loss of NaCl and neutral fluoranil, a black insoluble solid is produced that contains a mixture of unidentified products that are readily separated. This reaction demonstrates the ability to install an oxo ligand at a uranium center without change in the metal oxidation state through use of a redox active supporting ligand. A similar strategy was employed by Bart et al. to affect a 2-electron oxygen atom donation reaction in a U^{III}/U^{IV} transformation, in which one electron originates from a reduced bipyridyl ligand.[25]

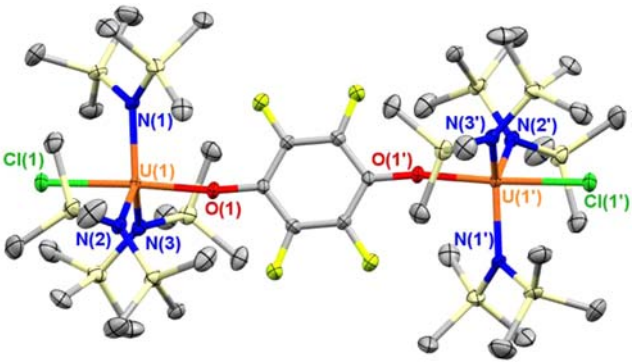

Figure 3. Thermal ellipsoid plot of **4** at 30% probability. Hydrogen atoms are omitted for clarity. Bond lengths (Å) and angles (deg): U(1)−Cl(1) 2.5852(19), U(1)−N(1) 2.166(7), U(1)−N(2) 2.189(6), U(1)−N(3) 2.189(6), U(1)−O(1) 2.145(5), O(1)−C(1) 1.353(8), Cl(1)−U(1)−O(1) 176.20(15), U(1)−O(1)−C(1) 169.3(5).

Analysis of Nitrite Reduction Mechanism. The formation of **1** from nitrite reduction proceeds through formal loss of NO, however, gas evolution was not directly observed in the reaction of $U^{V}Cl_2[N(SiMe_3)_2]_3$ with $NaNO_2$ due to the slow reactivity. The sluggish reactivity is attributed to the poor solubility of $NaNO_2$ in common organic solvents. However, the formation of **1** proceeded more rapidly with $AgNO_2$ resulting in observable gas evolution. The presence of nitric oxide in the evolved gas was confirmed by exposing the gaseous products to a solution of $Mo(N^tBuAr)_3$, Ar = 3,5-dimethylphenyl, using a system of nested vials. Capture of the gaseous reaction products led to formation of the known compound $Mo(N^tBuAr)_3(NO)$ as judged by IR spectroscopy.[37]

Analysis of the electrochemical potentials involved in the oxidation processes that lead to **1** and to the higher oxidation uranyl product suggests that the nitrite reduction reaction is electrochemically unfavorable. Electrochemistry measurements performed on $U^{V}Cl_2[N(SiMe_3)_2]_3$ in CH_2Cl_2 revealed a U(VI/V) couple of +0.91 V versus Fc/Fc^+,[19] which is greater than the reported aqueous standard reduction potential of the nitrite/nitric oxide couple of +0.52 V ($E^{\circ\prime}$ = +0.37 V) at pH 7.[38] This

dx.doi.org/10.1021/ja311057y | J. Am. Chem. Soc. 2013, 135, 511−518

difference is rationalized by electrochemical measurements on **1**, which show that the U(VI/V) couple is shifted to −0.35 V upon installation of the oxo-ligand corresponding to a stabilization of 1.26 V. Similarly, the amide ligand oxidation in **1** is beyond the observable window of +1 V, yet the second oxidation to form the uranyl product is spontaneous. The electrochemical data imply that these reactions are mediated by the thermodynamic driving force of the uranium−oxo bond formation rather than favorable electron transfer. To develop a detailed understanding of the thermochemistry involved in these reactions, we next studied species along reaction coordinate using DFT.

Theoretical Analysis of Mechanism. A computational investigation was carried out on the reaction pathway leading to complex **2**. DFT calculations were performed on $U^{V}ClF[N(SiMe_3)_2]_3$, several isomers of the intermediate $U^{V}(ONO)F[N(SiMe_3)_2]_3$, and $U^{VI}OF[N(SiMe_3)_2]_3$ (Figure 4). The

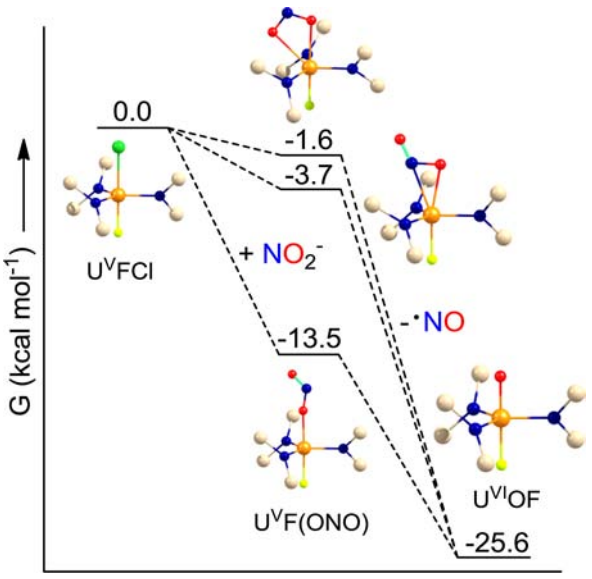

Figure 4. DFT calculated relative free energies for the proposed formation of **2** by reductive cleavage of nitrite. Methyl groups are removed for clarity.

synthesis of **2** implicates the initial associative formation of an unstable uranium−nitrite complex. In the proposed mechanism, homolytic cleavage of the N−O bond is accompanied by single electron transfer from the uranium(V) center, formally generating the uranium(VI)-oxo complex and nitric oxide. Given the potential for different possible nitrite coordination modes, we explored intermediates possessing κ^1-ONO, κ^2-O_2N, and κ^1-NO_2 linkages.

A minimum was found for each of the isomers, except for the κ^1-NO_2 complex, which converged to an η^2-ONO structure. Of the three isomers, the κ^1-ONO complex was found to be the lowest in energy. This complex exhibited a perturbation of the internal nitrite bond lengths with a proximal N−O bond of 1.383 Å and a distal N═O bond of 1.190 Å, indicative of alternating single and double bond character, as well as a short U−ONO bond length of 2.163 Å. The bonding arrangement in this intermediate is poised toward formation of a uranium−oxygen multiple bond and a nitrogen−oxygen multiple bond. In comparison, longer U−O bond lengths are noted in the other calculated isomers, with approximately equal N−O bond lengths indicative of delocalization. Only one structurally characterized U−ONO complex is known.[39] In that single example, the nitrite ion bridges two uranyl ions so there is no experimental data available for comparison to the calculated bond lengths.

The nitrite reduction mechanism proposed in the formation of **2** differs from that of nitrite reductases (NiR). In either the T2 copper center of the Cu−NiR enzymes or the heme-iron center of Fe−NiR,[40] nitrite is proposed to undergo one electron reduction to induce cleavage of the N−O bond. Similar reactivity has been demonstrated in synthetic iron complexes.[41,42] However, in general, reductive cleavage of NO_2^- is coupled to proton transfer with formation of metal−nitrosyl complexes and H_2O.[43] Recent work from the Solomon group suggests that CuNiR forms a κ^2-O_2N complex, which is protonated to form $Cu^{I}-(HNO_2)$ facilitating electron transfer to Cu^{II}−OH and nitric oxide.[44] The reactivity exhibited by uranium in the formation of **1** and **2** is fundamentally different from the reactivity of CuNiR, and is driven by formation of the U═O multiple bond. The U═O bond enthalpy is the primary driver for overcoming the barrier to electron transfer without the need for protonation. As axial, high valent uranium complexes are known to exert an inverse trans influence,[45−47] we next evaluated the electronic structures of our unique uranium(VI) compounds in detail.

Calculated Electronic Structures. A computational investigation of the of the isoelectronic complexes $U^{VI}F_2[N(SiMe_3)_2]_3^+$ (***1-F₂***), $U^{VI}OF[N(SiMe_3)_2]_3$ (***1-OF***), and $U^{VI}O_2[N(SiMe_3)_2]_3^-$ (***1-O₂***)[48] was performed to better understand the effect of axial ligand substitution on the electronic structure at uranium. The complex ***1-F₂*** has not yet been isolated, but electrochemical data supports its stability on that time scale. The frequency calculation performed on ***1-OF*** gave a U═O stretching mode of 905 cm^{-1} and a U−F stretching mode of 522 cm^{-1}, in reasonably good agreement with the experimentally observed values of 882 cm^{-1} and 504 cm^{-1}.

The optimized structures of the three complexes display a pronounced equatorial metal−ligand bond lengthening upon shifting from fluoro- to oxo-substitution, shown in Table 1.

Table 1. Comparison of Computationally Derived Bonding Metrics in *1-F₂*, *1-OF*, and *1-O₂*

	1-F₂	*1-OF*	*1-O₂*
U−N_{ave} calc'd (Å)	2.127	2.235	2.367
U−N_{ave} obs'd (Å)		2.208(2)	2.310(5)
U−N_{ave} MBO	1.266	0.970	0.734
%U in U−N_{ave} NBOs	18.68	15.21	10.15
%U in U−F/O NBOs	8.37	17.65	19.45
U natural charge	1.924	1.702	1.725
N_{ave} natural charge	−1.352	−1.481	−1.597
U($6p_z$) depopulation	−0.140	−0.158	−0.181

Similarly, the Mayer bond order (MBO) of the U−N bonds decreases with the increasing U−N bond lengths. These metrics are indicative of greater cis-destabilization by the oxo-ligands than the fluoride ligands. Cis-destabilization is recognized as a characteristic feature of an inverse trans influence (ITI),[47] though its precise origin is not completely understood.

NBO analysis showed a decreasing contribution of uranium AO character to the U−N bonding interactions upon substitution of fluoride with oxo ligands along with an increase in contribution of uranium AO character to axial U−F/O

dx.doi.org/10.1021/ja311057y | J. Am. Chem. Soc. 2013, 135, 511−518

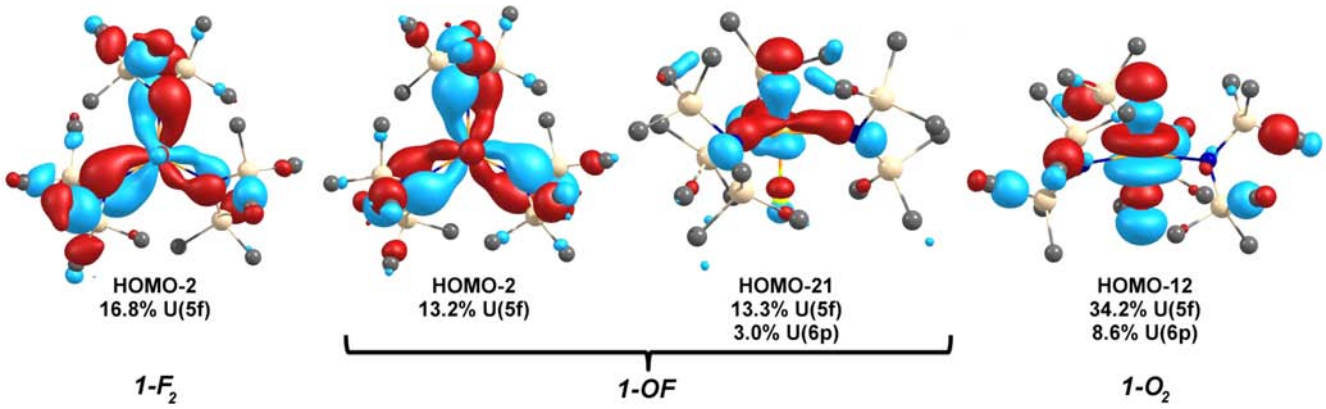

Figure 5. Comparison of occupied molecular orbitals of ***1-F***$_2$ (left), ***1-OF*** (center), and ***1-O***$_2$ (right) of greatest U(5f) orbital character.

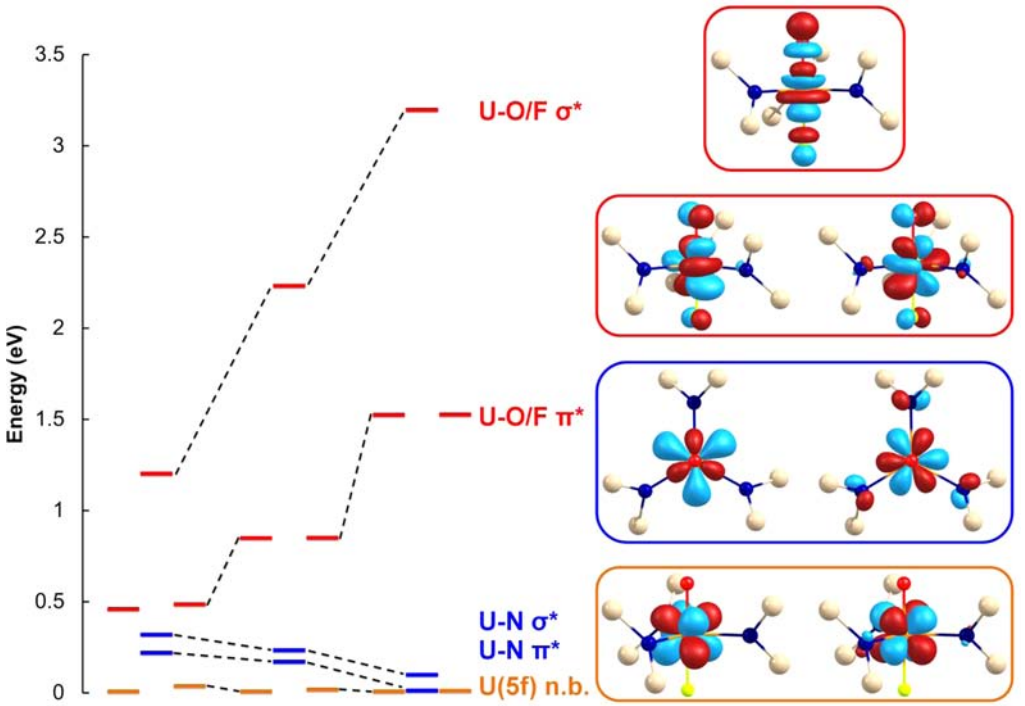

Figure 6. Correlation diagram between calculated LUMO to LUMO+6 orbitals for $U^{VI}F_2[N(SiMe_3)_2]_3^+$ (left), $U^{VI}OF[N(SiMe_3)_2]_3$ (middle), and $U^{VI}O_2[N(SiMe_3)_2]_3^-$ (right). Energies are plotted relative to the LUMO adjusted to 0 eV. Orbitals shown as degenerate pairs are not strictly degenerate, as each compound was optimized in C_1 rather than C_3 or D_3 symmetry. Orbitals shown are right are for ***1-OF***, with methyl groups removed for clarity.

bonding interactions. The natural charge on uranium decreases with oxo ligand substitution, whereas the natural charges on the amide nitrogen atoms become substantially more negative. These values suggest that the equatorial metal−ligand bonding is polarized away from the metal center with the stronger axial donor oxo ligands, suggestive of more ionic equatorial bonding. This means that the donation from the axial oxygen atom is much greater that the equatorial nitrogen atoms, rendering the equatorial bonding more ionic with increasing numbers of trans-oxo ligands. Therefore, the greater cis-destabilization exerted by the oxo ligands can largely be attributed to electro static effects due to the smaller covalent component to the equatorial bonding compared to the axial bonding. This is reflected in the structure of the complex $[Na(THF)_2][UO_2(N(SiMe_3)_2)_3]$, in which a Na^+ ion is directly bound to one uranyl-oxo ligand.[49] The Na^+ cation mediates the negative charge on the oxygen atom, and as a result the U−N bond lengths in this complex are shorter than those calculated for ***1-O***$_2$.

The nature of the axial bonding in these complexes was further examined through orbital analysis. Analysis of the uranium AO character in the occupied orbitals showed greater U(5f) character contributing to equatorial bonding interactions for ***1-F***$_2$, and substantially more U(5f) character contributing to axial bonding interactions in ***1-O***$_2$, illustrated in Figure 5. The complex ***1-OF*** exhibited intermediate behavior, with U(5f) character contributing approximately equally to axial and equatorial bonding interactions. Fragment molecular orbital analysis showed depopulation of the filled uranium semicore 6p AOs in all three complexes; however, whereas the $6p_x$ and $6p_y$ depopulation remained relatively constant, depopulation of the $6p_z$ orbital increased upon oxo substitution (Table 1). Notable U(6p) character was present in axial σ-bonding interactions (Figure 5), most pronounced in ***1-O***$_2$. Mixing of the uranium

dx.doi.org/10.1021/ja311057y | J. Am. Chem. Soc. 2013, 135, 511−518

$6p_z$ and $5f_z^3$ orbitals has been previously implicated in ITI stabilization of axial bonding.[46] The LUMO to LUMO+6 orbitals of each of the complexes are of primarily uranium(5f) character, as shown in Figure 6. Progressing from ***1-F₂*** to ***1-O₂***, there is a substantial increase in the axial U−O/U−F σ^* and π^* orbital energies, coupled to a decrease in the U−N σ^* and π^* orbital energies, shown in Figure 6. This trend in orbital energies also suggests that greater axial covalent interactions diminish equatorial U(5f)-ligand covalent interactions.

■ CONCLUSIONS

We have presented synthetic methods for replacement of uranium−chloride bonds with terminal uranium−oxygen multiple bonds, in which one-electron reductive cleavage of nitrite is facilitated by two different oxidation state changes − U^{IV}/U^{V}, and U^{V}/U^{VI}. We have also shown this reactivity can be driven by a ligand electron-reservoir that requires no change in metal oxidation state. This nitrite activation fundamentally differs from that of transition metal complexes as it proceeds at room temperature through a κ^1-ONO intermediate without the need for proton-assisted electron transfer, oxygen atom abstraction reagents such as phosphines, or photolysis. The trigonal bipyramidal structures exhibited by the uranium(VI)−oxo complexes are unique, as they allow for the installation of a variety of ligands trans to the U═O bond. As these reactions are driven primarily by the strong metal−oxo bond formation, we expect this protocol to be a general means to install an oxo ligand at a high valent uranium center through single electron oxidation.

■ EXPERIMENTAL SECTION

General Methods. All reactions and manipulations were performed under an inert atmosphere (N_2) using standard Schlenk techniques or in a Vacuum Atmospheres, Inc. Nexus II drybox equipped with a molecular sieves 13X/Q5 Cu−0226S catalyst purifier system. Glassware was oven-dried overnight at 150 °C prior to use. ^{1}H and ^{19}F NMR spectra were obtained on a Bruker DMX−300 Fourier transform NMR spectrometer at 300 MHz. UV−vis-NIR absorption measurements of complexes were performed using a PerkinElmer 950 UV−vis/NIR Spectrophotometer. One mm path length screw cap quartz cells were used with a blank measured before each run. The infrared spectra were obtained from 400−4000 cm^{-1} using a PerkinElmer 1600 series infrared spectrometer. Elemental analyses were performed at the University of California, Berkeley Microanalytical Facility using a PerkinElmer Series II 2400 CHNS analyzer.

Materials. Tetrahydrofuran, diethyl ether, dichloromethane, hexanes, and pentane were purchased from Fisher Scientific. The solvents were sparged for 20 min with dry N_2 and dried using a commercial two-column solvent purification system comprising columns packed with Q5 reactant and neutral alumina respectively (for hexanes and pentane), or two columns of neutral alumina (for THF, Et_2O, and CH_2Cl_2). Deuterated solvents were purchased from Cambridge Isotope Laboratories, Inc. and stored over potassium mirror overnight prior to use. Tetrafluoro-1,4-benzoquinone (Alfa Aesar) was recrystallized from toluene layered with hexanes at −25 °C prior to use. $Mo(N^tBuAr)_3$,[37] $U^{IV}Cl[N(SiMe_3)_2]_3$,[50] $U^{V}Cl_2[N(SiMe_3)_2]_3$,[19] $U^{V}ClF[N(SiMe_3)_2]_3$,[19] and $U^{IV}F[N(SiMe_3)_2]_3$[51] were prepared according to the published procedures. $NaNO_2$ (Sigma/Aldrich) was dried under vacuum at 150 °C overnight and $AgNO_2$ (Strem) was used as received.

Electrochemistry. Voltammetry experiments were performed using a CH Instruments 620D Electrochemical Analyzer/Workstation and the data were processed using *CHI* software v 9.24. All experiments were performed in an N_2 atmosphere drybox using electrochemical cells that consisted of a 4 mL vial, glassy carbon (3 mm diameter) working electrode, a platinum wire counter electrode, and a silver wire plated with AgCl as a quasi-reference electrode. The working electrode surfaces were polished prior to each set of experiments. All data were collected in a positive-feedback IR compensation mode.

X-ray Crystallography. X-ray intensity data were collected on a Bruker APEXII CCD area detector employing graphite-monochromated Mo−Kα radiation (λ = 0.71073 Å) at a temperature of 143(1)K. In all cases, rotation frames were integrated using *SAINT*,[52] producing a listing of unaveraged F^2 and $\sigma(F^2)$ values, which were then passed to the *SHELXTL*[53] program package for further processing and structure solution. The intensity data were corrected for Lorentz and polarization effects and for absorption using *TWINABS*[54] or *SADABS*.[55] The structures were solved by direct methods (*SHELXS-97*).[56] Refinement was by full-matrix least-squares based on F^2 using *SHELXL-97*.[56] All reflections were used during refinements. Non-hydrogen atoms were refined anisotropically and hydrogen atoms were refined using a riding model.

Synthesis of $U^{VI}OCl[N(SiMe_3)_2]_3$ (1). *(a). From $U^{V}Cl_2[N(SiMe_3)_2]_3$.* To a vial containing $U^{V}Cl_2[N(SiMe_3)_2]_3$ (75 mg, 0.09 mmol) stirring in 2 mL THF, $NaNO_2$ (52 mg, 0.95 mmol, 10.56 equiv) was added as a solid. After stirring 5 h, the volatiles were removed from the resulting green-black solution under reduced pressure. The black residue was dissolved in $(Me_3Si)_2O$, filtered through a Celite-packed coarse porosity fritted filter, and the volatiles were removed under reduced pressure yielding pure **1** as a black crystalline solid. Yield 54 mg, 0.07 mmol, 74%. Alternatively, performing this reaction under the same conditions with $U^{V}Cl_2[N(SiMe_3)_2]_3$ (33 mg, 0.04 mmol) and $AgNO_2$ (6.4 mg, 0.04 mmol, 1.00 equiv) yielded **2** following recrystallization from $(Me_3Si)_2O$ in two crops. Yield 23 mg, 0.03 mmol, 72%.

(b). From $U^{V}O[N(SiMe_3)_2]_3$. To a vial containing $U^{V}O[N(SiMe_3)_2]_3$ (85 mg, 0.12 mmol) stirring in 5 mL THF, $CuCl_2$ (78 mg, 0.58 mmol, 5.02 equiv) was added, resulting in an immediate color change to dark green. After stirring 30 min, the solution was filtered and volatiles were removed under reduced pressure. The black residue was extracted with pentane and recrystallized at −25 °C yielding **1** as a black crystalline solid. Yield 60 mg, 0.08 mmol, 67%.

(c). From $U^{IV}Cl[N(SiMe_3)_2]_3$. To a vial containing $U^{V}Cl[N(SiMe_3)_2]_3$ (117 mg, 0.16 mmol) stirring in 5 mL Et_2O, *N*-methylmorpholine-*N*-oxide (24 mg, 0.20 mmol, 1.32 equiv) was added resulting in a rapid color change to dark green. After stirring 45 min, the solution was filtered through Celite suspended in a glass pipet to remove residual *N*-methylmorpholine-*N*-oxide, and the volatiles were removed from the filtrate for an hour to ensure removal of volatile *N*-methylmorpholine. The black residue was dissolved in $(Me_3Si)_2O$, filtered through a Celite suspended in a glass pipet, and the volatiles were removed under reduced pressure to yield **1** as a black crystalline solid. Yield 61 mg, 0.08 mmol, 51%.

^{1}H NMR (benzene-d_6): δ 0.61 (27H), 0.55 (27H). IR (KBr, cm^{-1}): 2954 (w), 1404 (w), 1249 (s), 862 (m, $\nu_{U=O}$), 844 (s), 773 (s), 681 (w), 650 (s, $\nu_{U-N(amide)}$), 621 (s, $\nu_{U-N(amide)}$) (cm^{-1}). Elemental analysis found (calculated) for $C_{18}H_{54}ClN_3OSi_6U$: C, 28.42 (28.05); H, 7.18 (7.06); N, 5.16 (5.45).

Synthesis of $U^{VI}OF[N(SiMe_3)_2]_3$ (2). *(a). From $U^{V}ClF[N(SiMe_3)_2]_3$.* To a vial containing $U^{V}ClF[N(SiMe_3)_2]_3$ (50 mg, 0.07 mmol) stirring in 5 mL Et_2O, $AgNO_2$ (50 mg, 0.32 mmol, 5.00 equiv) was added as a solid. Occasional bubble formation from the surface of the suspended $AgNO_2$ was noted. After stirring 1 h, the volatiles were removed under reduced pressure and another 5 mL Et_2O was added, along with another addition of $AgNO_2$ (50 mg, 0.32 mmol, 5.00 equiv). After an additional stirring 3 h, the resulting dark green solution was filtered through Celite suspended in a pipet and volatiles were removed from the filtrate under reduced pressure. The resulting black residue was dissolved in $(SiMe_3)_2O$, filtered, and the volatiles were removed under reduced pressure yielding pure **2** as a black solid. Yield 35 mg, 0.05 mmol, 71%.

(b). From $U^{IV}F[N(SiMe_3)_2]_3$. Preparation was analogous to the procedure for the synthesis of **1**, with $U^{IV}F[N(SiMe_3)_2]_3$ (52 mg, 0.07 mmol) and *N*-methylmorpholine-*N*-oxide (9 mg, 0.08 mmol, 1.09 equiv), yielding **2** as a black solid. Yield 37 mg, 0.05 mmol, 71%.

dx.doi.org/10.1021/ja311057y | J. Am. Chem. Soc. 2013, 135, 511−518

^{1}H NMR (benzene-d_6): δ 0.56 (27H), 0.48 (27H). ^{19}F NMR (benzene-d_6): δ 586.8 (1F). IR (KBr, cm^{-1}): 2953 (w), 1400 (w), 1248 (s), 882 (m, $\nu_{U=O}$), 841 (s), 773 (s), 682 (w), 653 (s $\nu_{U-N(amide)}$), 620 (s, $\nu_{U-N(amide)}$), 504 (m, ν_{U-F}) (cm^{-1}). Elemental analysis found (calculated) for $C_{18}H_{54}FN_3OSi_6U$: C, 29.03 (28.67); H, 6.91 (7.22); N, 5.49 (5.57).

Synthesis of $U^{VI}OBr[N(SiMe_3)_2]_3$ (3). Preparation was analogous to the procedure for the synthesis of **1** (**b**), with $U^{V}O[N(SiMe_3)_2]_3$ (27 mg, 0.04 mmol) and $CuBr_2$ (20 mg, 0.09 mmol, 2.4 equiv). Recrystallization in minimal pentane at −21 °C yielded **3** as a black crystalline solid. Yield 27 mg, 90%. ^{1}H NMR (benzene-d_6): δ 0.62 (54H). IR (KBr, cm^{-1}): 2953 (w), 1385 (m), 1250 (s), 931(w), 859 (m, $\nu_{U=O}$) 843 (s), 773 (s), 682 (w), 651 (s, $\nu_{U-N(amide)}$), 622 (s, $\nu_{U-N(amide)}$) (cm^{-1}). Elemental analysis found (calculated) for $C_{18}H_{54}BrN_3OSi_6U$: C, 26.89 (26.52); H, 6.42 (6.68); N, 5.05 (5.16).

Synthesis of $\{U^{V}Cl[N(SiMe_3)_2]_3\}_2(\mu_2$-FA) (4). To a vial containing $U^{IV}Cl[N(SiMe_3)_2]_3$ (50 mg, 0.066 mmol) stirring in 5 mL Et_2O, tetrafluoro-*p*-quinone (fluoranil, FA) (6 mg, 0.033 mmol, 1.00 equiv) dissolved in minimal Et_2O was added, causing an immediate color change from pale tan to dark brown. After stirring 15 min, the volatiles were removed under reduced pressure. The black residue was dissolved in pentane and filtered through Celite suspended in a glass pipet. Removal of volatiles under reduced pressure yielded **4** as a dark red-brown solid. Yield 46 mg, 0.027 mmol, 82%. ^{1}H NMR (47 °C, benzene-d_6): δ −0.74 (54H), −1.16 (54H). The room temperature ^{1}H NMR spectrum displayed multiple broad, overlapping peaks between 0 to −3 ppm. ^{19}F NMR (benzene-d_6): −138.8 (4F). IR (KBr, cm^{-1}): 3138 (m), 2958 (w), 2925(w), 1491(s), 1400 (s), 1299 (w), 1251(m), 1033 (m), 984 (m), 845 (s), 775 (w), 651 (m), 620 (m) (cm^{-1}). Elemental analysis found (calculated) for $C_{42}H_{108}Cl_2F_4N_6O_2Si_{12}U_2{\cdot}0.5C_6H_{14}$: C, 31.43 (31.20); H, 6.09 (6.69); N, 4.76 (4.85).

Synthesis of $U^{V}O[N(SiMe_3)_2]_3$. *From $U^{IV}Cl[N(SiMe_3)_2]_3$.* To a vial containing $U^{IV}Cl[N(SiMe_3)_2]_3$ (50 mg, 0.07 mmol) in 3 mL THF, $AgNO_2$ (10 mg, 0.07 mmol, 0.98 equiv) was added as a solid. Mild bubble formation was noted along with a color change to red. After 6 h, the solution was filtered through Celite suspended in a glass pipet, and volatiles were removed under reduced pressure. The resulting red residue was extracted with pentane, filtered, and recrystallized at −21 °C to yield $U^{V}O[N(SiMe_3)_2]_3$ as a red solid. Yield: 24 mg, 0.03 mmol, 49%.

From 4. To a vial containing **4** (56 mg, 0.03 mmol) stirring in 5 mL THF, $NaNO_2$ (5 mg, 0.07 mmol, 2.19 equiv) suspended in minimal THF was slowly added. After stirring 12h, the resulting orange-red solution had a significant amount of black solid suspended in it. The solution was filtered through Celite suspended in a glass pipet and volatiles were removed under reduced pressure. Extraction with pentane, filtration, and recrystallization yielded $U^{V}O[N(SiMe_3)_2]_3$ as a red solid. Yield: 32 mg, 0.04 mmol, 65%.

Characterization data for $U^{V}O[N(SiMe_3)_2]_3$ was consistent with previously reported data.[24]

■ ASSOCIATED CONTENT

Ⓢ Supporting Information

X-ray crystallographic files (CIFs), computational details, UV−vis-NIR data, and electrochemistry data. This material is available free of charge via the Internet at http://pubs.acs.org.

■ AUTHOR INFORMATION

Corresponding Author

*E-mail: schelter@sas.upenn.edu.

Notes

The authors declare no competing financial interest.

■ ACKNOWLEDGMENTS

We thank the University of Pennsylvania for financial support. We thank the NSF for support of the X-ray diffractometer (CHE-0840438) and computing cluster (CHE-0131132). This work used the Extreme Science and Engineering Discovery Environment (XSEDE), which is supported by National Science Foundation grant number OCI-1053575. We thank Dr. Nick Piro for his suggestion to use $Mo(N^tBuAr)_3$, Ar = 3,5-dimethylphenyl, to detect $NO_{(g)}$. We also thank Prof. Christopher R. Graves (Albright College) and Prof. Richard A Andersen (U.C. Berkeley) for helpful discussions.

■ REFERENCES

(1) Merkle, A. C.; Lehnert, N. *Dalton Trans.* **2012**, *41*, 3355.
(2) Kumar, M.; Dixon, N. A.; Merkle, A. C.; Zeller, M.; Lehnert, N.; Papish, E. T. *Inorg. Chem.* **2012**, *51*, 7004.
(3) Woollard-Shore, J. G.; Holland, J. P.; Jones, M. W.; Dilworth, J. R. *Dalton Trans.* **2010**, *39*, 1576.
(4) Kujime, M.; Izumi, C.; Tomura, M.; Hada, M.; Fujii, H. *J. Am. Chem. Soc.* **2008**, *130*, 6088.
(5) Chuang, W.-J.; Lin, I. J.; Chen, H.-Y.; Chang, Y.-L.; Hsu, S. C. N. *Inorg. Chem.* **2010**, *49*, 5377.
(6) Tsai, F.-T.; Kuo, T.-S.; Liaw, W.-F. *J. Am. Chem. Soc.* **2009**, *131*, 3426.
(7) Tsai, F.-T.; Chen, P.-L.; Liaw, W.-F. *J. Am. Chem. Soc.* **2010**, *132*, 5290.
(8) Suslick, K. S.; Watson, R. A. *Inorg. Chem.* **1991**, *30*, 912.
(9) Yamaji, M.; Hama, Y.; Miyazaki, Y.; Hoshino, M. *Inorg. Chem.* **1992**, *31*, 932.
(10) Hoshino, M.; Iimura, Y.; Konishi, S. *J. Phys. Chem. A* **1992**, *96*, 179.
(11) Owen, T. M.; Rohde, J.-U. *Inorg. Chem.* **2011**, *50*, 5283.
(12) Fox, A. R.; Bart, S. C.; Meyer, K.; Cummins, C. C. *Nature* **2008**, *455*, 341.
(13) Arnold, P. L. *Chem. Commun.* **2011**, *47*, 9005.
(14) Hayton, T. W. *Dalton Trans.* **2010**, *39*, 1145.
(15) Bart, S. C.; Anthon, C.; Heinemann, F. W.; Bill, E.; Edelstein, N. M.; Meyer, K. *J. Am. Chem. Soc.* **2008**, *130*, 12536.
(16) Kosog, B.; La Pierre, H. S.; Heinemann, F. W.; Liddle, S. T.; Meyer, K. *J. Am. Chem. Soc.* **2012**, *134*, 5284.
(17) Fortier, S.; Kaltsoyannis, N.; Wu, G.; Hayton, T. W. *J. Am. Chem. Soc.* **2011**, *133*, 14224.
(18) Mills, D. P.; Cooper, O. J.; Tuna, F.; McInnes, E. J. L.; Davies, E. S.; McMaster, J.; Moro, F.; Lewis, W.; Blake, A. J.; Liddle, S. T. *J. Am. Chem. Soc.* **2012**, *134*, 10047.
(19) Lewis, A. J.; Nakamaru-Ogiso, E.; Kikkawa, J. M.; Carroll, P. J.; Schelter, E. J. *Chem. Commun.* **2012**, *48*, 4977.
(20) Cantat, T.; Graves, C. R.; Scott, B. L.; Kiplinger, J. L. *Angew. Chem., Int. Ed.* **2009**, *48*, 3681.
(21) Arney, D. S. J.; Burns, C. J. *J. Am. Chem. Soc.* **1995**, *117*, 9448.
(22) Zi, G.; Jia, L.; Werkema, E. L.; Walter, M. D.; Gottfriedsen, J. P.; Andersen, R. A. *Organometallics* **2005**, *24*, 4251.
(23) Fortier, S.; Wu, G.; Hayton, T. W. *J. Am. Chem. Soc.* **2010**, *132*, 6888.
(24) Fortier, S.; Brown, J. L.; Kaltsoyannis, N.; Wu, G.; Hayton, T. W. *Inorg. Chem.* **2012**, *51*, 1625.
(25) Kraft, S. J.; Walensky, J.; Fanwick, P. E.; Hall, M. B.; Bart, S. C. *Inorg. Chem.* **2010**, *49*, 7620.
(26) Arnold, P. L.; Pécharman, A.-F.; Love, J. B. *Angew. Chem., Int. Ed.* **2011**, *50*, 9456.
(27) *CRC Handbook of Chemistry and Physics*; 86th ed.; Lide, D. R., Ed.; CRC Press: Boca Raton, FL, 2005−2006.
(28) Burns, C. J.; Smith, W. H.; Huffman, J. C.; Sattelberger, A. P. *J. Am. Chem. Soc.* **1990**, *112*, 3237.
(29) Andersen, R. A. *Inorg. Chem.* **1979**, *18*, 1507.
(30) Barnhart, D. M.; Burns, C. J.; Sauer, N. N.; Watkin, J. G. *Inorg. Chem.* **1995**, *34*, 4079.
(31) Arnold, P. L.; Patel, D.; Blake, A. J.; Wilson, C.; Love, J. B. *J. Am. Chem. Soc.* **2006**, *128*, 9610.
(32) Roberts, B. P.; Winter, J. N. *J. Chem. Soc., Chem. Commun.* **1978**, 545.

(33) Arnold, P. L.; Hollis, E.; White, F. J.; Magnani, N.; Caciuffo, R.; Love, J. B. *Angew. Chem., Int. Ed.* **2011**, *50*, 887.
(34) Downs, A. J.; Gardner, C. J. *J. Chem. Soc., Dalton Trans.* **1984**, 2127.
(35) Straka, M.; Kaupp, M. *Chem. Phys.* **2005**, *311*, 45.
(36) Joubert, P.; Bougon, R.; Gaudreau, B. *Can. J. Chem.* **1978**, *56*, 1874.
(37) Laplaza, C. E.; Odom, A. L.; Davis, W. M.; Cummins, C. C.; Protasiewicz, J. D. *J. Am. Chem. Soc.* **1995**, *117*, 4999.
(38) Averill, B. A. *Chem. Rev.* **1996**, *96*, 2951.
(39) Sun, D.; Zhang, N.; Xu, Q.-J.; Huang, R.-B.; Zheng, L.-S. *Inorg. Chem. Commun.* **2010**, *13*, 859.
(40) Williams, P. A.; Fulop, V.; Garman, E. F.; Saunders, N. F. W.; Ferguson, S. J.; Hajdu, J. *Nature* **1997**, *389*, 406.
(41) Harris, T. D.; Betley, T. A. *J. Am. Chem. Soc.* **2011**, *133*, 13852.
(42) Villar-Acevedo, G.; Nam, E.; Fitch, S.; Benedict, J.; Freudenthal, J.; Kaminsky, W.; Kovacs, J. A. *J. Am. Chem. Soc.* **2011**, *133*, 1419.
(43) Leferink, N. G. H.; Han, C.; Antonyuk, S. V.; Heyes, D. J.; Rigby, S. E. J.; Hough, M. A.; Eady, R. R.; Scrutton, N. S.; Hasnain, S. S. *Biochemistry* **2011**, *50*, 4121.
(44) Ghosh, S.; Dey, A.; Sun, Y.; Scholes, C. P.; Solomon, E. I. *J. Am. Chem. Soc.* **2008**, *131*, 277.
(45) Denning, R. In *Complexes, Clusters and Crystal Chemistry*; Springer: Berlin/Heidelberg: 1992; Vol. *79*, p 215.
(46) Denning, R. G. *J. Phys. Chem. A* **2007**, *111*, 4125.
(47) O'Grady, E.; Kaltsoyannis, N. *J. Chem. Soc., Dalton Trans.* **2002**, 1233.
(48) Compound numbers in italics denote computational model compounds.
(49) Burns, C. J.; Clark, D. L; Donohoe, R. J.; Duval, P. B.; Scott, B. L.; Tait, C. D. *Inorg. Chem.* **2000**, *39*, 5464.
(50) Turner, H. W.; Andersen, R. A.; Zalkin, A.; Templeton, D. H. *Inorg. Chem.* **1979**, *18*, 1221.
(51) Stewart, J. L. *Tris[bis(trimethylsilyl)amido]uranium: Compounds with Tri-, Tetra-, and Pentavalent Uranium*; Lawrence Berkeley Lab., 1988.
(52) Bruker (2009) SAINT. Bruker AXS Inc., Madison, Wisconsin, USA.
(53) Bruker (2009) SHELXTL. Bruker AXS Inc., Madison, Wisconsin, USA.
(54) Sheldrick, G. M. (2008) TWINABS. University of Gottingen, Germany.
(55) Sheldrick, G. M. (2007) SADABS. University of Gottingen, Germany.
(56) Sheldrick, G. M. *Acta Crystallogr.* **2008**, *A64*, 112.